General Disclaimer

One or more of the Following Statements may affect this Document

- This document has been reproduced from the best copy furnished by the organizational source. It is being released in the interest of making available as much information as possible.

- This document may contain data, which exceeds the sheet parameters. It was furnished in this condition by the organizational source and is the best copy available.

- This document may contain tone-on-tone or color graphs, charts and/or pictures, which have been reproduced in black and white.

- This document is paginated as submitted by the original source.

- Portions of this document are not fully legible due to the historical nature of some of the material. However, it is the best reproduction available from the original submission.

Experimental Investigation of Capillary Propellant Control Devices for Low Gravity Environments

Volume I - Summary Report

June 1970

Prepared Under Contract NAS8-21259 for

George C. Marshall Space Flight Center
Marshall Space Flight Center, Alabama 35812

MARTIN MARIETTA CORPORATION

MCR-69-585

Contract NAS8-21259

Experimental Investigation of Capillary Propellant Control Devices for Low Gravity Environments

Volume I: Summary Report

June 1970

Prepared for

George C. Marshall Space Flight Center
Marshall Space Flight Center, Alabama 35812

Approved by

Howard L. Paynter
Program Manager

Martin Marietta Corporation
Denver, Colorado 80201

FOREWORD

This report was prepared by the Martin Marietta Corporation, Denver, Colorado, under Contract NAS8-21259, Experimental Investigation of Capillary Propellant Control Devices for Low-Gravity Environments. It includes work done under an earlier study, Contract NAS8-20837, Design, Fabrication, and Testing of Subscale Propellant Tanks with Capillary Traps. Both programs were conducted for the George C. Marshall Space Flight Center of the National Aeronautics and Space Administration. The period of performance for the first program was from June 26, 1967 to March 15, 1968. The second study covered the period from May 2, 1968 to June 30, 1970.

The work was administered under the technical direction of Mr. Leon J. Hastings of the Propulsion and Vehicle Engineering Laboratory of the George C. Marshall Space Flight Center. A color-film summary of the experimental results can be obtained from Mr. Hastings.

CONTENTS

I. INTRODUCTION

Surface tension devices are one of the more promising techniques for the low-g storage and transfer of cryogens and non-cryogens. A screen or perforated plate is configured within the storage tank to orient single-phase fluid at the proper outlet (drain or vent) and provide continuous control of the bulk liquid (minimize c.g. offset). Ullage pressure supports the liquid position while surface tension maintains separation of the fluid phases by stabilizing the liquid-ullage interface at the foraminous material. The simplicity and inherent reliability of these passive systems make them prime candidates for many of the future space missions.

The purpose of this experimental drop tower program was to obtain engineering data to advance the state-of-the-art of capillary designs for liquid propellant orientation and control.

II. OBJECTIVES

The program objectives were to investigate via drop tower tests: (1) the liquid/gas interfacial stability provided by perforated plate and square-weave screen under an acceleration acting normal to the foraminous surface; (2) various passive schemes for preventing the passage of settled propellants;

(3) the liquid/gas interfacial stability provided by perforated plate and screen under an acceleration acting parallel to the foraminous surface; and (4) liquid filling of capillary annuli and the removal of undersired vapor pockets during filling.

III. TEST APPARATUS AND PROCEDURE

The experimental program was conducted in Martin Marietta's 2.1-sec drop tower that uses the encapsulated test cell principle. The 34.0-in dia test cell housing the experiment, power supply, lights, and 16-mm Milliken camera, falls within the 42.0-in dia, 116-in long drag shield during the 75-ft unguided drop. Tests were conducted at near-constant axial accelerations from near-zero* to 0.055-g (nominal) during the entire free-fall interval. near-constant lateral accelerations ranging from 0.047- to 1.51-g (nominal) were provided for lesser durations during some of the drops. NEG'ATOR** constant-torque motors are used to provide the controllable and repeatable axial and lateral accelerations.

The transparent test specimens (containing the foraminous material) were mounted on the test cell platform in view of the camera, as shown in Figure 1. The platform was positioned parallel to the top of the test cell so that it was perpendicular

---

* The near-zero condition is estimated to be less than 10^{-5} g. It is achieved by evacuating the space between the test cell and drag shield to a level of 5 mm Hg absolute (maximum).

** Tradename. Hunter Spring Co., Hatfield, Pennsylvania.

to the capsule's vertical centerline. The test cell was balanced so its centerline coincided with a vertical line through its attachment with the drag shield (prior to drop initiation). The NEG'ATOR motors (for axial acceleration) were attached to the bottom of the test cell (on its centerline) so that the force acted along this line during test.

The capsule assembly used for the majority of the more than 300 drop tests is pictured in Figure 2. The test cell was not used for the lateral acceleration tests because it afforded an insufficient lateral travel distance. Instead the platform, pictured in Figure 3, was mounted directly to the bottom section of the drag shield. The test specimens were, therefore, subjected to a slight axial drag force (on the order of 10^{-4}g) which was negligible compared to the lateral accelerations mentioned earlier. For these tests, results were photographed using the reflector arrangement shown. The test specimens moved toward the reflector, viewed by the camera, during their 15-in travel distance.

The test liquids, methanol, carbon tetrachloride, Freon-TF, and chloroform, were selected since they possessed the desired physical properties to simulate a wide range of propellants. The properties considered for similitude were the kinematic surface tension, β, and the liquid-to-solid contact angle, θ. The

values for the test liquids and propellants (see Table 1) show that the β range of the test liquids, 4.15- to 10.1 x 10^{-4} ft^3/sec^2, covers the oxidizers and extends to the fuels. It does not cover the monopropellants, such as hydrazine. The test liquids were assumed to be totally-wetting ($\theta = 0^o$) to the test specimens, as are most liquid propellants to aluminum, titanium, and stainless steel, materials common to storage tanks. A small trace of dye was added to the test liquids to provide better photographic quality.

IV. EXPERIMENTAL RESULTS

The results for each of the different test phases are presented separately in the following paragraphs.

A. Hydrostatic Liquid/Gas Interface Stability (Acceleration Normal to Foraminous Surface)

The objective was to determine the ability of perforated plate and square-weave-screen to stabilize the liquid/gas interface at the foraminous surface under axisymmetric, constant accelerations acting normal to the surface. Single, flat, foraminous samples were positioned 4- or 6-in from the bottom of 10-in tall glass cylinders (4.970-in ID). A total of 77 drop tests was made under accelerations ranging from 0.0013 to 0.055g. The majority of tests were made with the test liquid filling the bottom portion of the cylindrical specimen and covering the

Table I Physical Properties of Test Liquids and Storable Propellants

PROPELLANTS	TEMPERATURE (°C)	DENSITY, ρ (lb_m/ft^3)	SURFACE TENSION, σ ($\times 10^3$ lb_f/ft)	KINEMATIC SURFACE TENSION, σ/ρ ($\times 10^6$ ft^3/sec^2)	CONTACT ANGLE, θ (deg)*	VISCOSITY, μ ($\times 10^5$ lb_m/ft-sec)
Fuels:						
Aerozine-50	20	55.5(a)	2.07(a)	12.0	0 to 2(a)	0.581(b) at 21°C
MMH		54.6(c) at 24°C	2.35(c) at 20°C	13.8		0.518(c) at 25°C
UDMH	20	49.4(d)	1.92(d)	12.5	0 to 0.75(d)	0.37(e)
MHF-5	20	63.0(f)	2.64(g)	13.5		1.64(h) at 16°C
JP-4	20	48.4(i)	1.55(d)	10.3		0.712(e)
Hydrogen	-254	4.48(d)	0.162(d)	11.6	0(j)	
Oxidizers:						
Nitrogen Tetroxide	20	90.6(d)	1.88(d)	6.68		0.277(e) at 21°C
Nitric Acid (Fuming)	20	97.2(a)	3.01(a)	9.98	0 to 3(a,d)	0.918(e)
Chlorine Triflouride	11.7	115.5(k)	1.70(k)	4.74		0.292(l)
Oxygen	-183	71.2(d)	0.908(d) at -192°C	4.10	0(j)	
Monopropellants:						
Hydrogen Peroxide (90%)	20	87.0(a)	5.41(a)	20.0	1 to 2(a)	0.849(e)
Hydrazine	20	62.4(a)	4.33(a)	22.3	0 to 2(a)	0.654(e)
Test Liquids						
Methanol	20	49.4(i)	1.55(i)	10.1	0(i)	0.453(m)
Carbon Tetrachloride	20	99.6(i)	1.84(i)	5.95	0(i)	0.645(n)
Freon-TF	20	98.6(i)	1.27(i)	4.15	0(i)	0.468(n)

*Contact angles for storables are for Pyrex, 6061-T6 polished aluminum, 301 polished stainless steel, and ASTM 8348-59T Grade 6 polished titanium alloy; for test liquids, they represent contact with Pyrex.

References:

(a) *Summary Report: Studies of Interfacial Surface Energies.* NASA CR-54175. Harris Research Laboratories, Rockville, Maryland, December 1964.

(b) *Storable Liquid Propellants for Titan II.* LRP 198 (Rev A). Aerojet-General Corp, Sacramento, California, September 30, 1960.

(c) R. W. Lawrence: *Handbook of Properties of UDMH and MMH.* 1292. Aerojet-General Corp, Sacramento, California, May 1958.

(d) W. C. Reynolds, M. A. Saad, and H. M. Satterlee: *Capillary Hydrostatics and Hydrodynamics at Low g.* T.R. LG-3. Mechanical Engineering Dept, Stanford University, Stanford, California, September 1964.

(e) *Liquid Propellants Handbook.* Battelle Memorial Institute, Columbus, Ohio, October 1958.

(f) *Handbook of Chemistry and Physics.* 44th Edition. Chemical Publishing Co, Cleveland, Ohio.

(g) *Final Report: Evaluation of Propellant Containment and Venting Devices for Zero-Gravity Applications.* AFRPL-TR-65-118. Bell Aerosystems Co, Buffalo, New York, June 1965.

(h) S. Tannenbaum et al: *Advanced Propellants Investigation for Pre-Packaged Liquid Engine.* RMD 5046-F. Thiokol Chemical Corp, Danville, New Jersey, June 10, 1965.

(i) W. J. Masica et al: *Hydrostatic Stability of the Liquid-Vapor Interface in a Gravitational Field.* NASA TN D-2267. May 1964.

(j) C. E. Siegert et al: *Behavior of the Liquid-Vapor Interface in a Gravitational Field.* NASA TN D-2658. February 1965.

(k) P. A. Friedman and J. Winkler: *Properties of Fluorine and Fluorine-Based Propellants.* TM-0444-64-8. Martin Marietta Corporation, Denver, Colorado, July 1964.

(l) A. H. Banks, A. Davies, and A. J. Rudge: "Determination of Surface Tension and Viscosity of Liquid Chlorine Trifluoride." *J. Chemical Society,* 732-5, 1953.

(m) *Chemical Engineering Handbook.* Third Edition. Edited by J. H. Perry. McGraw-Hill, Inc, New York City, New York, 1950.

(n) E. J. Bennett and G. J. Roewe, Jr.: *Cleaning Electronic and Space Apparatus with "Freon" Precision Cleaning Agent.* Solvent Bulletin FST-4. E. I. duPont de Nemours & Co, Inc, Wilmington, Delaware.

upper-surface of the flat barriers. The liquid cover ranged from 1/8- to 1/4-in; two drops were made at a liquid cover of about one-in.

The criteria used to evaluate the film results were that the pore was stable:

1) when no gas was ingested through the barrier during the drop interval; or

2) when the liquid/gas interface configuration showed no time dependence during the drop.

The first criterion was used for the higher acceleration test conditions; the second, at the 0.0013g condition. For the latter, a single pore only was evaluated; for the higher-g conditions, barriers with numerous openings were used. The single pore necessitated study of its liquid/gas interface to determine stability.

The test results for bare, uncoated perforated plate are presented in Figure 4. The pore radii tested are plotted against the ratio of kinematic surface tension (β)-to-the average acceleration. The straight line tends to separate the stable and unstable regions and is based on a Bond number (Bo) of 0.84 where Bo is:

$$Bo = \frac{ar^2}{\beta} \qquad (1)$$

and a is acceleration and r is pore radius. The data show good verification of the Bo criterion for hydrostatic pore stability and tend to support a critical value of 0.84.

The data for square-weave screen are presented in Figure 5. Considerably fewer tests were conducted for screen and results are less conclusive. Again, the data verify the Bo criterion, based on one-half the screen opening. (The pore size, as presented, is one-half the opening of the square-weave.) The critical Bo = 0.45 is less than that for perforated plate since the interface stability is reduced by a lateral acceleration due to its complex geometry. Although the acceleration vector is applied normal to the screen, a lateral component also acts on the interface due to the weaving process whereby warp and shute wires are crimped over and under each other. The resultant pore geometry is, therefore, three-dimensional.

The single-sample-experiment technique was used to estimate the accuracy of the Bo determination. The following Bo uncertainty limits were established for the three nominal test conditions: $\pm$6.4% at 0.055g; $\pm$6.2% at 0.020g; and $\pm$5.6% at 0.0013g.

B. Damping Tests

The tests were similar to those described in Part A except that the initial liquid level was below the foraminous barriers. The liquid was 2.0-in from the bottom surface of the barrier for the lowest axisymmetric settling acceleration (0.022g) and 3.0-in for the two higher accelerations (0.031 and 0.040g). The corresponding h/R values* are 0.806 and 1.205, respectively. The

* The h term is the vertical distance from the liquid to the bottom surface of the foraminous barrier; R is the cylindrical test specimen radius.

liquid level was chosen so that the settling liquid contacted the barrier within one-sec (after capsule release) to allow at least one-sec to observe damping. The tests were conducted over a settling Bo range from 30.4 to 135.0 to yield the desired settling condition (analogous to the period following engine shutdown when drag forces tend to position liquid away from the liquid drain port) characterized by liquid flow along the wall of the cylindrical specimen and also in a central column. The axial acceleration was applied at drop initiation, therefore, the liquid surface was flat at initiation of settling.

The objective was to determine the ability of different foraminous material to damp and control the liquid during settling. Wall flow always contacted the barrier before the central liquid column; therefore, some tests were made with an annular-ring deflector to interrupt the wall flow. The majority of the more than 100 drops were made without the deflector.

The barriers evaluated included: single and double perforated plate; single and double square-weave screen; multi-tube and single tube configurations; and single layer Dutch-twill cloth. The open-to-closed area ratio (ξ) for flow normal to the surface of the foraminous material ranged from zero to 0.575. Two barrier configurations had an $\xi = 0$. The Dutch-twill cloth affords no open area to flow due to its intricate weave that provides an internal capillary network only for flow through

the material. The double perforated plate barrier had the two plates positioned so that they also provided no open area to flow. The 0.087-in thick aluminum plates were separated by an 0.087-in gap.

The maximum impingement velocity for the columnar flow data can be described as

$$v_c = K_c \quad (2ah)^{\frac{1}{2}}, \qquad (2)$$

with K_c determined from Figure 6. The K_c value varied from 0.495 to 0.601 for methanol and carbon tetrachloride at the two different liquid-level conditions ($h/R \approx 0.806$ and $h/R \approx 1.205$). The Freon-TF results ranged from $0.622 \leq K_c \leq 0.945$, which was considerably higher. The central liquid formation, shape, and flow characteristics were different for the Freon-TF. Following the formation of a central liquid hump, the dome appeared to settle toward the barrier. Subsequent wave phenomena caused the liquid column to neck down and accelerate as a smaller-dia. dome. This type of motion yielded instantaneous surface accelerations at barrier impact that were greater than those for methanol and carbon tetrachloride, particularly at the two lower acceleration test conditions (see Figure 6).

A film analyzer and recorder (Boscar Model N-1) was used to measure displacement of wall flow and columnar flow as a function of drop test time. Movement was translated into coded signals

that were stored and displayed digitally. A vertical scale, photographed with each test, was used to calibrate the machine readings. The test interval was determined by film frame count and timing marks (20 per second) on the film. Velocity data were obtained by graphical differentiation of the flow histories.

The performance of the barriers was categorized against the following damping regimes (see Figure 7):

A) No liquid passes through the barrier;

B) Some liquid (relatively little) passes during wetting of the barrier by liquid settling along the wall of the cylindrical specimen;

C) The dome of the liquid column either penetrates the barrier, resulting in a sessile globule, or recedes completely;

D) The central liquid mass penetrates the barrier as one or two columns that pinch off and stay above the barrier, but no additional liquid passes;

E) Similar to D, but the columns are not completely pinched off;

F) A considerable amount of liquid passes through most of the barrier surface, and there is a number of columns (streamers);

G) A massive amount of liquid passes through the barrier with no apparent damping.

Regime A is most desired; B and C also show good damping. Regimes F and G display negligible damping. The D and E categories separate the damped and undamped regimes (see Figure 7).

The damping performance of each barrier was correlated with the impingement Weber number, We, at the pores of the barrier using the relationship

$$We = v_c^2 r/\beta ; \qquad (2)$$

where v_c is the central liquid column impingement velocity and β is the kinematic surface tension. The pore radii (r) for perforated-plate and square-weave barriers are one-half the open-pore dimension; but for Dutch Twill, an effective radius of one-half the pore openings (based on absolute micron rating) was used (see Table 2).

The damping performance for the single and double perforated plate and the single square-weave and Dutch-twill screen barriers are presented in Figure 8. The single-plate and square-weave results are for tests made with no wall-flow deflector. Some liquid (Category B) always passed through the single plate and screen during wetting of the barrier by the wall flow. The double-plate and Dutch-twill results are for tests conducted both with and without the wall-flow deflector. As opposed to the single plate and square-weave results, there was no noticeable difference for tests with or without the deflector. The double

Table 2 Perforated Plate and Screen Barriers

BARRIER NO.	MATERIAL*	PLATE THICKNESS (in.)	PORE DIA. (in.)	PORE LAYOUT FIG.	PORE LAYOUT ℓ (in.)	ε†	ADDITIONAL DESCRIPTION
1	Aℓ	0.087	0.125	29	0.250	0.176	
1A	Aℓ	0.032	0.125	29	0.250	0.176	
1B	Aℓ	0.125	0.125	29	0.250	0.176	
2	Aℓ	0.087	0.187	29	0.375	0.153	
2A	Aℓ	0.032	0.187	29	0.375	0.153	
2B	Aℓ	0.125	0.187	29	0.375	0.153	
3	Aℓ	0.087	0.253	29	0.250	0.155	
4	Aℓ	0.087	0.376	29	0.750	0.141	
5	Aℓ	0.087	0.271	29	0.500	0.178	Tubes (L/D = 4.41) protrude 0.25 in. above plate.
6	Aℓ	0.087	0.183	29	0.375	0.145	Tubes (L/D = 4.02) protrude 0.25 in. above plate.
7	Aℓ	0.087	0.065	Centered - Single Pore		0.030	Tubes are 3 in. long and open-ended. Upper end is flush with with top of plate.
8	Aℓ	0.087	0.937	Centered - Single Pore		0.035	Screen tube (200x1400 mesh) is 2.75 in. long and closed at bottom. Upper end is flush with top of plate.
9	Aℓ	0.087	0.256	29	0.625	0.105	
10	Aℓ	0.087	0.256	30	0.313	0.575	
11	Aℓ	0.087	0.191	29	0.469	0.106	
12	Aℓ	0.087	0.191	30	0.250	0.430	
13	Aℓ	0.087	0.253	30	0.625	0	Used with Barrier 9; barriers are separated by 0.087 in. (Fig. 31)
14	Aℓ	0.087	0.187	30	0.469	0	Used with Barrier 11; barriers are separated by 0.087 in. (Fig. 31)
15	Aℓ	0.087	0.271	29	0.500	0.178	Same as for Barrier 5, but with tubes flush with bottom of plate.
16	Aℓ	0.087	0.183	29	0.375	0.145	Same as for Barrier 6, but with tubes flush with bottom of plate.

*Aℓ = aluminum.

†Ratio of open-to-closed area (flow normal to barrier).

BARRIER.NO.	MATERIAL*	WEAVE	MESH SIZE	PORE OPENING (in.)	WIRE DIA. (in.)	ε†
17	S.S.	Dutch Twill	325 x 2300	0.000473		0
18	S.S.	Dutch Twill	200 x 1400	0.000709		0
19	S.S.	Dutch Twill	165 x 800	0.001380		0
20	S.S.	Square	50 x 50	0.010000	0.010	0.250
21	S.S.	Square	30 x 30	0.020300	0.013	0.371
22§	S.S.	Square	12 x 12	0.065300	0.018	0.608
23	S.S.	Square	12 x 12	0.065300	0.018	0.608
24§	S.S.	Square	30 x 30	0.020300	0.013	0.371
28	S.S.	Square	100 x 100	0.005500	0.0045	0.302
29	S.S.	Square	200 x 200	0.002900	0.0021	0.336
30	S.S.	Dutch Twill	30 x 250	0.002760		0
31	S.S.	Dutch Twill	24 x 110	0.00551		0

*S.S. = stainless steel.

†Ratio of open-to-closed area (flow normal to barrier).

§Two layers of screen separated by an 0.087-in. spacer.

Note: Pore dimensions for the square-weave screen are per the supplier (Pyramid Screen Co.); the effective pore sizes for Dutch twill are based on abs. micron ratings (as specified by the Western Filter Company and Kressilk Products, Inc.).

plate and twilled cloth barriers provided good damping for all tests, as shown.

The single-plate results, are for an open-to-closed area ratio (ξ) equal to, or less than, 0.176. Poor damping categories F and G were observed for additional single-plate tests at two higher ξ numbers, 0.430 and 0.575. A drastic performance difference was also observed for tests made with and without the wall-flow deflector. For example, the same plate barrier that showed Category B damping at We = 0.626 (no deflector) displayed Category E damping at We = 0.463 (with deflector). Similarly, another barrier showed Category C damping at We = 1.691, but Category F damping at a lower We number (We = 0.806) with wall-flow deflector.

The Dutch-twill screen displayed Category A damping for most tests (see Figure 8). The small pore radii resulted in relatively low We numbers in comparison to the other barriers. It is interesting that the C damping category observed at We = 0.018 for the twilled cloth compared to that for the square-weave screen (see Figure 8). This tends to suggest that possibly the performance for the two different weaves would be comparable at corresponding We numbers; one real advantage of the twilled cloth is its smaller pore radii.

The double-plate and Dutch-twill barriers performed best. These differ from the other barriers in that neither affords an open area to the settled liquid flow (see Table 2). Rather, they

cause the flow to take a tortuous path through the barrier and at the same time provide a capillary network to aid and maintain wetting. The tortuousity factor and the ability to wet the barrier are pertinent design considerations for good damping performance.

There was no apparent effect on barrier performance due to plate thickness for the thicknesses tested (including those for the multi-tube barriers with the tubes flush with the bottom of the plate, see Table 2). The performance results for the multi-tube configuration, in which the tubes protruded below the plate, were comprable to those for the single-perforated-plate barriers. The performance of the double-layer square-weave screen was comparable to the single-layer.

The method for single-sample experiments was used to provide some measure of reliability of test results. Following the manner discussed earlier, the uncertainty limits (based on the cylinder radius R) at the three nominal low-g test conditions were as follows for the settling Bo: $\pm$5.5% at 0.040g; $\pm$5.9% at 0.031g; and $\pm$6.5% at 0.022g. The impingement We uncertainty limit is estimated to be less than $\pm$10.8%.

C. Hydrostatic Liquid/Gas Interface Stability (Acceleration Parallel to Foraminous Surface)

The purpose of this experimental phase of the study was to evaluate the hydrostatic interface stability at the surface of

perforated plates and screens over a range of accelerations parallel to the material (with a near-zero acceleration normal to the material).

As mentioned in Chapter III, activation of the lateral accelerator mechanism was delayed until about 0.75 sec. after capsule release for two reasons: (1) the distance (15-in) limited the lateral travel interval to less than one sec; and (2) near-weightless interface shapes (minimum surface energy conditions) would be attained in the pores of the material before the lateral travel was begun.

The foraminous material evaluated (see Table 3) included: (1) perforated plate; (2) square-weave screen; and (3) twilled cloth. A total of 139 lateral acceleration tests was made for the test situation pictured in Figure 9. As with the hydrostatic testing discussed in part (A), a liquid cover above the upper-surface of the barrier of about 1/4-in, or less, was used to provide repeatable data. The liquid cover compensated for the overall capsule misalignment, variations in the NEG'ATOR force, and undesirable perturbations caused by hoisting the capsule to its drop height and by releasing the capsule.

Referring to Figure 9, the near-constant lateral acceleration (a_L) produces a hydrostatic head (ΔP_h) across the material which is a maximum between stations 1 and 2:

Table 3 Barriers Used in Lateral Acceleration Tests

(15.0 in. of Lateral Travel)

BARRIER	DESCRIPTION	r (ft)	OPEN-TO-CLOSED AREA (%) - ξ *
1	Aluminum plate with a 90° array of 1/32-in.-diameter straight holes on 1/16-in. centers.	0.00137	22.2
2	Aluminum plate with a 90° array of 1/16-in.-diameter straight holes on 1/8-in. centers.	0.00268	22.7
3	Aluminum plate with a 90° array of 1/16-in.-diameter straight holes on 3/16-in. centers.	0.00259	9.5
4	Aluminum plate with a 90° array of 1/8-in.-diameter straight holes on 3/8-in. centers.	0.00521	11.5
5	Stainless steel plate with a 60° array of 0.026-in.-diameter cone holes on 0.042-in. centers.	0.00108	36.2
6	100 x 100-mesh stainless steel square weave screen.	0.000246	34.8
7	50 x 50-mesh stainless steel square weave screen	0.000442	28.1
8	30 x 250-mesh stainless steel Dutch twill weave screen.	0.000145	0
9	24 x 110-mesh stainless steel Dutch twill weave screen.	0.000180	0

*Flow normal to the surface of the material.

Note: Pore dimensions presented for screen were measured for the square-weave (microscope) and Dutch-twill (bubble-point).

$$\Delta P_h = \rho \frac{a_L}{g_c} h_{12} \qquad (3)$$

where h_{12} is measured, as shown. A ratio of this pressure difference to the capillary pressure differential;

$$\Delta P_c \approx \frac{\sigma}{r} \cos \theta \qquad (4)$$

where r is pore radius and θ is the liquid-to-solid contact angle, yields an acceleration-to-capillary force ratio similar to the Bo expression. This ratio defined here as the ϕ number, may be written as;

$$\phi = \frac{a_L h r}{\beta} \qquad (5)$$

where cos θ is assumed as unity.

In addition to this dimensionless number, an additional parameter, similar to the Galileo number and denoted here as Ga, was identified through the use of the Buckingham Pi theorem along with a number of other dimensionless groups. This modified Ga number is defined as;

$$G_a = \frac{a_L d^2 h}{\nu^2} \qquad (6)$$

where d is pore dia and ν is kinematic viscosity.

The data show a relatively strong dependence on the ϕ number and the open-to-closed area ratio (ξ); a somewhat weaker relationship to the Ga number was noted.

Two types of interface instability were observed ... continuous and non-continuous. The latter was characterized by gas

breakthrough followed by apparent stability, or vice versa. It is believed that this resulted because of variations in the lateral acceleration. In addition, the calculated accelerations showed that the value usually decreased slightly with lateral travel distance due to frictional drag and resistance caused by irregularities in the near-parallel guide rails. As mentioned in Chapter III, lateral travel histories were obtained from a neon bulb/magnetic reed switch arrangement. The lateral travel time between reed switch stations was determined from marks on the 16mm film (20 marks per sec). Average accelerations were calculated from these data.

The method used to calculate the dimensionless numbers was as follows. When the interface was stable, the highest calculated acceleration (between reed stations) was used. When the interface was unstable, either the lowest acceleration (for continuous breakthrough) or the average acceleration to the reed switch following breakdown (non-continuous) was used.

The test data correlation of Ga versus $\emptyset$ number is presented in Figures 10 to 13 for plate and screen. The straight lines plotted for each figure delineate the stable and unstable interface results. The ξ values (see Table 3) are presented, along with the slope of the line (m) and the intercept on the Ga ordinate (B). The rather weak dependence on the Ga number is evident.

The critical Ø number for the perforated plate ranged from 1.2 to 1.7 (ξ = 36.2%) and 2.1 to 2.5 ($9.5 \leq \xi \leq 22.7\%$). The square-weave data ($28.1 \leq \xi \leq 34.8\%$) tend to support a critical Ø number range of 0.85 to 0.95, whereas the twilled cloth results show the critical Ø number is about 1.1.

The results presented in Figures 10 and 11 are plotted in Figure 14 to dramatize the effect of ξ on interface stability. This lower stability (critical Ø number) with increased ξ may be explained by referring to Figure 9. As mentioned earlier, the tests were made with liquid 1/4-in, or less, above the barriers to ensure that the material was wetted before the capsule was dropped. Upon initiation of the lateral acceleration, this liquid tended to follow the arrows shown in the figure. The amount of liquid above the barrier that moved down into and through the pores was strongly influenced by the open area of the barrier. The momentum of this liquid must be dissipated by viscous shear and by the capillary differential pressure force at the pores. As ξ increases, therefore, the interface stability decreases.

An analysis similar to that mentioned in the previous tests was performed to estimate the accuracy of test results. The uncertainty values for the Ga and Ø numbers are less than $\pm$7.75% except for the square-weave screen where the uncertainty is less than $\pm$13.0%. The greater uncertainty for the square-weave is

due to its greater variation in screen pore opening (as measured using a microscope with a calibrated stage).

D. Filling Capillary Annuli

The operational principle of these surface tension systems was mentioned in Chapter I. Single phase fluid (liquid) may be drained from a storage tank during low-g provided that: (1) the annulus of the capillary system contains liquid only; and (2) the bulk liquid reservoir is in contact with the annulus. When these two criteria are met, liquid will drain from the reservoir, into the annulus, and out the tank, on demand.

The experimental studies discussed in the previous parts of this chapter dealt with establishing criteria for the selection of foraminous materials and the design of devices to provide liquid positioning and control. These design criteria should be adequate to satisfy the requirement that the bulk liquid will contact the liquid flow annulus. The objective of the work described here was to evaluate capillary refilling of annuli and the impact on system designs.

A total of twenty-one drop tests was made using simple, cylindrical and spherical glass specimens with a concentric screen liner to provide a liquid flow annulus (constant gap size). Dutch-twill (200 x 1400 mesh) and square-weave (40 and 100 mesh)

screen were used. The test liquids were methanol and chloroform.* Zero and negative-g (0.003- to 0.022-g) conditions were provided at various liquid-to-container volume ratios from 17 to 89.4%. The negative acceleration vector tended to aid annulus filling.

The rather limited test data (see Table 4) show that: (1) wicking of the Dutch-twill cloth prohibited capillary pumping to fill the annuli; and (2) complete filling of annuli formed by square-weave screen was achieved but only for liquid-to-container volume ratios less than, or equal to, 47%. The Dutch Twill wicking phenomenon (internal capillary network) was discussed earlier. The incomplete filling of the square-weave screen system was caused by the bulk liquid reservoir reorienting from 1-g to its low-g minimum energy condition and wetting the screen at a rate greater than afforded the annuli by capillary pumping.

Test data for the spherical test specimen under zero- and 0.0216-g (negative) are presented in Figure 15 alongwith predicted fill times based upon the equation of mass continuity

$$\nabla \cdot \underset{\sim}{v} = 0 \qquad (7)$$

*Chloroform was used only in this phase of the experimental program. Its physical properties at 20°C are: ρ = 93.0 lb_m/cu. ft; σ = 1.85 x 10^{-3} lb_f/ft; β = 6.41 x 10^{-4} ft^3/sec^2; and μ = 3.89 x 10^{-4} lb_m/ft-sec. The properties for methanol are listed in Table 1.

Table 27 Summary of Data on Annulus Filling

RUN	TEST SPECIMEN*	LIQUID	ACCELERATION (g)	SCREEN MESH	FULL OF LIQUID (%)	ANNULUS FILLED	TIME REQUIRED TO FILL ANNULUS (sec)
1	1	Methanol	0	100	22.3	Yes	1.34
2	1	Methanol	-0.0036	100	22.3	Yes	1.30
3	1	Methanol	-0.0180	100	22.3	Yes	1.05
4	1	Methanol	0	100	45.4	Yes	1.04†
5	1	Methanol	-0.0030	100	45.4	Yes	0.97†
6	1	Methanol	-0.0147	100	45.4	Yes	0.845†
7	1	Methanol	0	100	45.4	Yes	1.07§
8	1	Methanol	-0.0030	100	45.4	Yes	1.00§
9	1	Methanol	-0.0147	100	45.4	Yes	0.845§
10	1	Methanol	0	100	28.3	Yes	1.42
11	1	Methanol	0	100	70.9	No	
12	1	Methanol	0	100	89.4	No	
13	2	Methanol	0	200x1400	25.0	No	
14	2	Methanol	0	200x1400	50.0	No	
15	2	Methanol	0	200x1400	75.0	No	
16	3	Chloroform	0	40	17.0	Yes	1.44¶
17	3	Chloroform	0	40	25.0	Yes	1.22¶
18	3	Chloroform	0	40	47.0	Yes	0.875
19	3	Chloroform	-0.0216	40	17.0	Yes	1.40¶
20	3	Chloroform	-0.0216	40	25.0	Yes	1.105¶
21	3	Chloroform	-0.0216	40	47.0	Yes	0.735

*Test specimen designations: 1 = Horizontal Cylinder
Diameter = 3.44 in.
Annulus Gap = 0.125 in.
Length = 2.31 in.
2 = Horizontal Cylinder
Diameter = 4.875 in.
Annulus Gap = 0.125 in.
Length = 4.25 in.
3 = Sphere
Diameter = 8.46 in.
Annulus Gap = 0.11 in.

†Experimental package handled with considerable care to avoid sloshing liquid on the screen.

§Experimental package handled so that liquid contacted the entire screen before the drop.

¶Liquid expulsion (0.35 lb_m/sec) initiated after 0.9 sec of drop time.

and the equation for the conservation of momentum

$$\frac{\partial \underset{\sim}{v}}{\partial t} + (\underset{\sim}{v} \cdot \nabla) \underset{\sim}{v} + \frac{\nabla P}{\rho} = \underset{\sim}{a} + \text{viscous term.} \qquad (8)$$

We assumed one-dimensional flow in the spherical annulus and accounted for viscous effects via a friction-factor approach. The viscous term is assumed to be

$$\text{Viscous term} = - \frac{4f}{D} \cdot \frac{\rho v^2}{2} , \qquad (9)$$

where the hydraulic diameter, D, is four times the flow area divided by the wetted perimeter. Since the flow area in the spherical annulus is the lateral area of the frustum of a cone (half the slant height times the perimeter), the hydraulic diameter is:

$$D = 2\ell. \qquad (10)$$

The friction factor is assumed to be inversely proportional to the Reynolds number:

$$4f = \frac{K}{Re} = \frac{K\nu}{v\ell} . \qquad (11)$$

Since there is no exact solution to act as a guide to the proper value for K as there is with flow inside a tube (where K = 64), we made the assumption of one-dimensional flow in the spherical annulus (see Figure 16). This is expressed by

$$\underset{\sim}{v} = \underset{\sim}{v}i_{\theta}, \text{ where } \chi(t) < \theta < \gamma(t). \qquad (12)$$

The mean height of the bulk liquid interacts with the annulus

at $\theta = \chi(t)$. The liquid/vapor interface inside the annulus is at $\theta = \gamma(t)$.

The continuity equation, (7), can be expressed in spherical coordinates as

$$\frac{\partial}{\partial \theta} (v \sin \theta) = 0, \tag{13}$$

or as

$$v(\theta,t) \sin \theta = v\left[\gamma(t),t\right] \sin \gamma(t). \tag{14}$$

The momentum equation becomes:

$$\frac{\partial v}{\partial t} + \frac{v}{R}\left(\frac{\partial v}{\partial \theta}\right) + \frac{1}{\rho R}\left(\frac{\partial p}{\partial \theta}\right) = -g \sin \theta - \frac{K\nu}{4\ell^2} v. \tag{15}$$

Now, using the continuity result, Eq (14), the momentum equation, Eq (15), can be solved for pressure as:

$$\frac{\partial p}{\partial \theta} = -\rho R\left\{\frac{\frac{\partial}{\partial t}\left[v(\gamma,t) \sin \gamma\right]}{\sin \theta} - \frac{v^2(\gamma,t) \sin^2 \gamma \cos \gamma}{R \sin^3 \theta} + \frac{\frac{K\nu}{4\ell^2} v(\gamma,t) \sin \gamma}{\sin \theta} - g \sin \theta\right\}, \tag{16}$$

which integrates to

$$p(R,\gamma,t) - p(R,\chi,t) = -\rho R\left(\left\{\frac{\partial}{\partial t}\left[v(\gamma,t) \sin \gamma\right] + \frac{K\upsilon}{4\ell^2} v(\gamma,t) \sin \gamma\right\} \ell n\left(\frac{\tan \frac{\chi}{2}}{\tan \frac{\gamma}{2}}\right) + \frac{v^2(\gamma,t)}{2R}\left(\frac{\sin^2 \gamma}{\sin^2 \chi} - 1\right) + g(\cos \chi - \cos \gamma)\right). \tag{17}$$

The liquid pressure is related to the ullage pressure by the surface-tension expression

$$p(R,\gamma,t) = p_{ullage} - \sigma\left(\frac{1}{R_1} + \frac{1}{R_2}\right), \quad (18)$$

where R_1 and R_2 are the principal radii of curvature. In approximation:

$$R_1 \approx \frac{\ell}{2}\ ; \quad (19)$$

$$R_2 \approx -R \tan \gamma. \quad (20)$$

Now, by assuming that the liquid pressure at $\Theta = \chi$ is approximately equal to the ullage pressure -- i.e., that

$$p(R,\chi,t) \approx p_{ullage}, \quad (21)$$

we do not need to consider the fluid dynamics inside the spherical screen nor the interaction with flow in the annulus. Thus, the pressure difference is simply

$$p(R,\chi,t) - p(R,\gamma,t) \approx \sigma\left(\frac{2}{\ell} - \frac{1}{R \tan \gamma}\right); \quad (22)$$

and the assumption of one-dimensional flow allows us to relate velocity and the position of the annulus interface by the kinematic condition

$$v(\gamma,t) = R\,\frac{d\gamma}{dt}\ . \quad (23)$$

Consequently, Eq (17) can be written:

$$\frac{d^2\gamma}{dt^2} + \left(\frac{d\gamma}{dt}\right)^2 \cot\gamma + \frac{K\nu}{4\ell^2}\left(\frac{d\gamma}{dt}\right) = \frac{\frac{g}{R}(\cos\gamma - \sin\gamma) + \frac{\sigma}{\rho R^3}\left(\frac{2R}{\ell} - \cot\gamma\right) + \frac{1}{2}\left(\frac{\sin^2\gamma}{\sin^2\chi} - 1\right)\left(\frac{d\gamma}{dt}\right)^2}{\sin\gamma\,\ell\,n\left(\frac{\tan\frac{\gamma}{2}}{\tan\frac{\chi}{2}}\right)}, \quad (24)$$

where the angles γ and χ are interrelated by mass continuity.

The volume of bulk liquid (inside the screen) is

$$V_L = \frac{\pi}{3}(R - \ell)^3\left[2 - \cos\chi\,(3 - \cos^2\chi)\right], \quad (25)$$

and the volume in the annulus is

$$V_A = \frac{2\pi}{3}R^3\left[1 - \left(1 - \frac{\ell}{R}\right)^3\right](1 - \cos\gamma). \quad (26)$$

Mass continuity requires that:

$$V_A + V_L = \text{constant} = \left(V_A + V_L\right)\Big|_{t=0}; \quad (27)$$

and since the ratio of liquid volume-to-container volume can be written

$$V_R = \frac{V_A + V_L}{\frac{4\pi R^3}{3}}, \quad (28)$$

Eq (27) can be written as:

$$\left(1 - \frac{\ell}{R}\right)^3\left[2 - \cos\chi\,(3 - \cos^2\chi)\right] + 2\left[1 - \left(1 - \frac{\ell}{R}\right)^3\right](1 - \cos\gamma) = 4V_R, \quad (29)$$

which is a cubic equation for cos χ in terms of γ, as shown by:

$$\cos^3\chi - 3\cos\chi + 2\left\{1 - \cos\gamma\left[1 - \left(1 - \frac{\ell}{R}\right)^3\right] - 2V_R\right\} = 0. \quad (30)$$

The proper root of Eq (30) is

$$\cos\chi = 2\cos\left(\frac{\cos^{-1}\left\{2V_R + \left[1 - \left(1 - \frac{\ell}{R}\right)^3\right]\cos\gamma - 1\right\} + 4\pi}{3}\right). \quad (31)$$

Writing non-dimensional versions of Eq (24) and (31) in terms of the following:

$$\frac{t_{fill}}{t'} = f\ (\alpha, Bo, S, V_R), \quad (32)$$

where:

$$t' = \left(\frac{\sigma}{\rho R^3}\right)^{-\frac{1}{2}} \quad ; \quad (33)$$

$$\alpha = \frac{\ell}{R} \quad ; \quad (34)$$

$$Bo = \frac{gR^2\rho}{\sigma} \quad ; \quad (35)$$

$$S = \left(\frac{\rho v^2}{\sigma R}\right)^{\frac{1}{2}} \quad ; \quad (36)$$

$$V_R = \frac{V_L}{V_C} \quad ; \quad (37)$$

with

$$\bar{t} = \frac{t}{t'} \quad , \quad (38)$$

we have

$$\frac{d^2\gamma}{d\bar{t}^2} + \left(\frac{d\gamma}{d\bar{t}}\right)^2 \cot\gamma + \frac{KS}{4\alpha^2}\left(\frac{d\gamma}{dt}\right) = \frac{Bo(\cos\gamma - \cos\chi) + \frac{2}{\alpha} - \cot\gamma + \frac{1}{2}\left(\frac{d\gamma}{d\bar{t}}\right)^2\left(\frac{\sin^2\gamma}{\sin^2\chi} - 1\right)}{\sin\gamma\,\ell n\left(\frac{\tan\frac{\gamma}{2}}{\tan\frac{\chi}{2}}\right)} \quad (39)$$

and

$$\cos \chi = 2 \cos \left(\frac{\cos^{-1} \left\{ 2V_R + \left[1 - (1-\alpha)^3 \right] \cos \gamma - 1 \right\} + 4\pi}{3} \right) . \tag{40}$$

These two equations can be solved numerically by integration from the initial conditions ($t = 0$, $\gamma = \gamma_o$, and $\chi - \chi_o$) to the desired final conditions of a filled annulus ($\gamma - \pi$) to yield the fill time such that

$$\bar{t} \Big|_{\gamma = \pi} .$$

This fill time is determined by the initial conditions and the parameters in Eq (32).

Equations (39) and (40) were programed for computer solution. Data for the filling of the spherical annulus (Table 4) were input, and the friction factor was chosen as the tube flow factor ($K = 64$). Figure 16 compares the theoretical and test results. The comparison is somewhat inappropriate since outflow from the sphere was initiated after 0.9 sec, whereas the theory does not model this outflow; however, the agreement is relatively good and tends to prove the theory.

The maximum pressure difference the wetted screen can support can be approximated by

$$\Delta P \lesssim \frac{4\sigma}{r} \tag{41}$$

where the factor of 4 (rather than 2) is due to the presence of the two liquid surfaces (a thin liquid film cover). The capillary

pressure difference due to the annulus interface is approximately

$$P_A - P_L \approx \frac{2\sigma}{\ell} \tag{42}$$

where the subscripts A and L refer to the annulus (gas) and liquid, and ℓ is the annulus gap width. Thus, if capillary pumping is to break the liquid film on the screen and permit the annulus to be filled, then the gap must be such that

$$\frac{2\sigma}{\ell} > \frac{4\sigma}{r} \tag{43}$$

or $\ell < r/2$. This criterion is restrictive and impractical for Dutch-twill cloth because of its effective pore radius (on the order of 5 to 50 microns). Therefore, perforated plate and/or square-weave screen should be used. In addition, it may be necessary to use deflection baffles to prevent, or at least slow, wetting of the foraminous material during reorientation of the bulk liquid reservoir.

V. CONCLUSIONS AND RECOMMENDATIONS

A. Conclusions

The quantitative and qualitative test results presented in this report are applicable to the design of capillary systems.

The primary objective of the study was to determine and verify, via drop tower experiments, pertinent dimensionless parameters needed to more efficiently design passive systems. The Bo number was verified as the important scaling parameter for hydrostatic stability when the acceleration vector is normal to the foraminous material. A form of the Bo number (the $\emptyset$ number) and a modified Ga number were determined as the pertinent scaling parameters for liquid/gas interface stability when the acceleration vector acts parallel to the foraminous material.

For interface stability evaluations, in which a wetted barrier was desired, the majority of tests were made with the liquid 1/4-in. or less above the perforated material. This liquid cover was needed to compensate for misalignment of the drop capsule and test specimen and to keep the barrier wetted at the initiation of the drop test. The motion of this liquid cover under an imposed acceleration must be damped by the capillary pressure difference at the pores. The presence of this momentum contribution tends to reduce the stability criteria. This effect was not thoroughly evaluated during the program, except for slight variations in the liquid cover. It would be desirable to obtain additional data for a greater range of liquid cover depths.

Different passive schemes were evaluated with regard to their ability to damp and control liquid under axisymmetric settling. Their passive function is similar to a one-way check valve in

that they must permit the passage of pressurization gas and liquid in one direction but prevent the passage of liquid in the opposite direction. The two schemes that showed best performance were the double-plate and the Dutch-twill configurations.

Various damping categories (A thru G) are presented as a function of the liquid's impingement We number for the various schemes. The damping was categorized from A, no liquid passage through the barrier, to G, no apparent damping. The results are qualitative since certain parameters, such as the open-to-closed area ratio, were not thoroughly evaluated.

Drop tower test results are also presented that qualitatively document complete and incomplete filling of capillary annuli formed by perforated plate (or screens) and the tank wall to provide a path for liquid draining. Methods are presented to provide complete liquid filling and refilling of capillary annuli.

The results of the program show that the designer must have a good understanding of the performance requirements for the capillary device so that he can correctly specify a particular foraminous material. When ordering Dutch-twill screen, it is usually preferred to specify a particular pressure to be retained (or bubble point) and the desired mesh size; specifying pressure retention, by itself, is usually not adequate. For example, if the material is to be used to form an annular flow passage for

liquid draining, the designer is also concerned about flow loss and wicking characteristics. Different foraminous materials can satisfy a specified pressure-retention requirement; however, their flow loss and wicking characteristics may be different. (Square-weave screens and perforated plates will not wick, as will the Dutch-twill.)

Similarly, different diameter wires may be used in a given kind of square-weave screen that has only been specified according to mesh size; accordingly, different samples may have different open dimensions and open-to-closed area ratios. The number of holes and type of hole pattern in a perforated plate will also affect its open-area ratio.

As still another example, merely specifying the pressure-retention requirement is not adequate if the foraminous material is to be used to provide damping. As discussed in Chapter IV-B, the type of weave is equally important if a screen is to be used, since having a tortuous flow path and the ability to effect complete wetting of the material are definite requirements for good liquid damping.

In general, for any kind of screen the specified pressure retention and mesh size must be consistent. The same is true when purchasing perforated plates; the designer should specify hole size, tolerance limits, and the array (hole pattern). The

hole size specified must be consistent with the pressure-retention requirement.

B. Recommendations

There is no single capillary design which is best for all possible storage applications. Rather, different configurations are preferred for different tank sizes and shapes, types of propellants (cryogens or non-cryogens), propellant properties (surface tension, density, and viscosity), environmental conditions during prelaunch, launch, and low-g storage, and propellant-orientation, control, and supply requirements.

It would, therefore, be a difficult, if not an impractical task, to conduct a general investigation that would document criteria directly applicable to all possible capillary designs. For example, during this experimental program more than 300 drop tests were conducted and still more data are desired to provide additional quantitative results.

The approach recommended for designing capillary systems for sub-critical, non-cryogen storage is to use the criteria presented here to yield a preliminary design which is then verified and modified, as required, using sub-scale and full-scale bench tests and drop tower studies. On the other hand, orbital tests may be needed to verify capillary designs for low-g, cryogen storage.

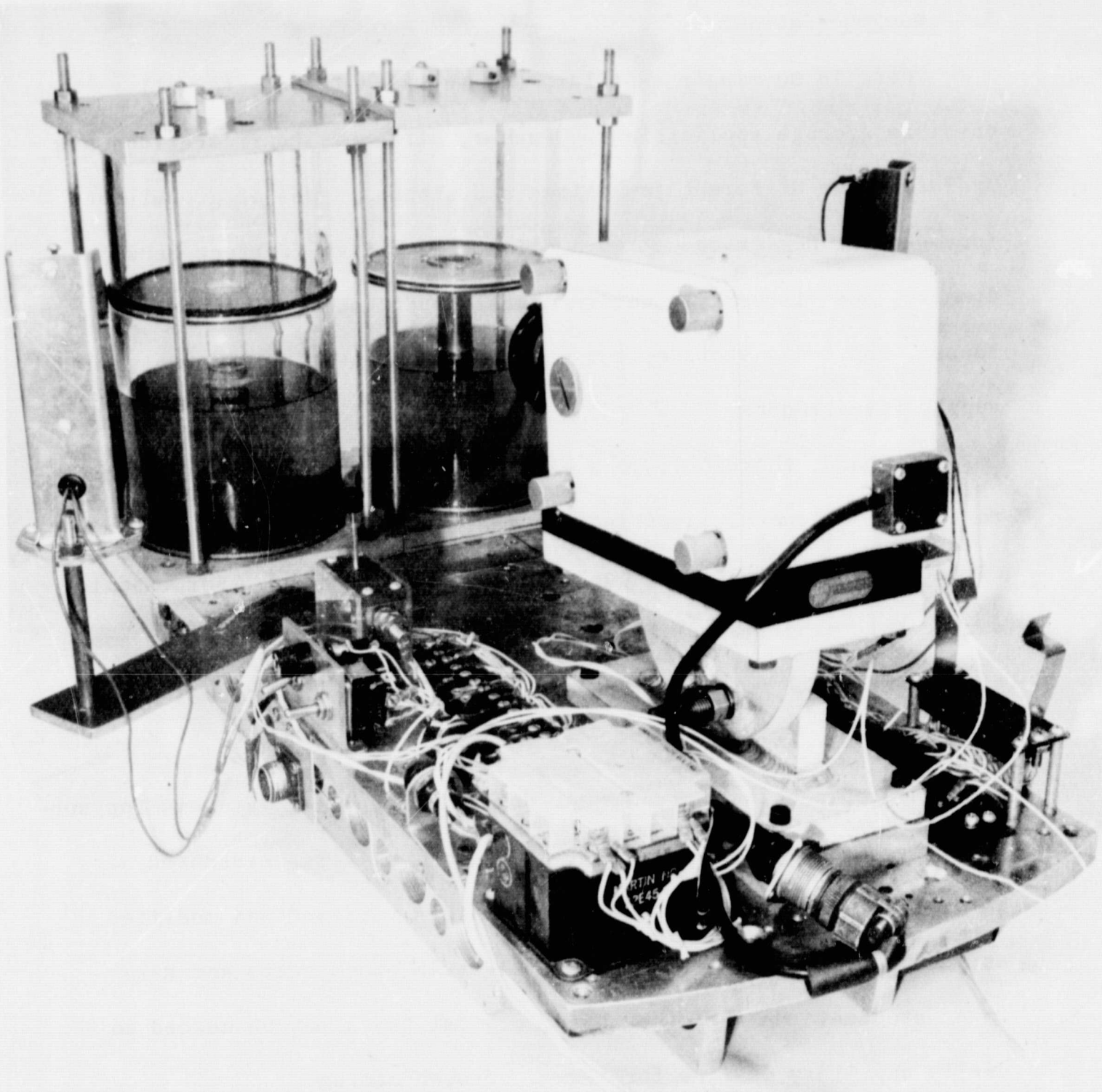

Fig. 1 Test Specimen Setup (Typical)

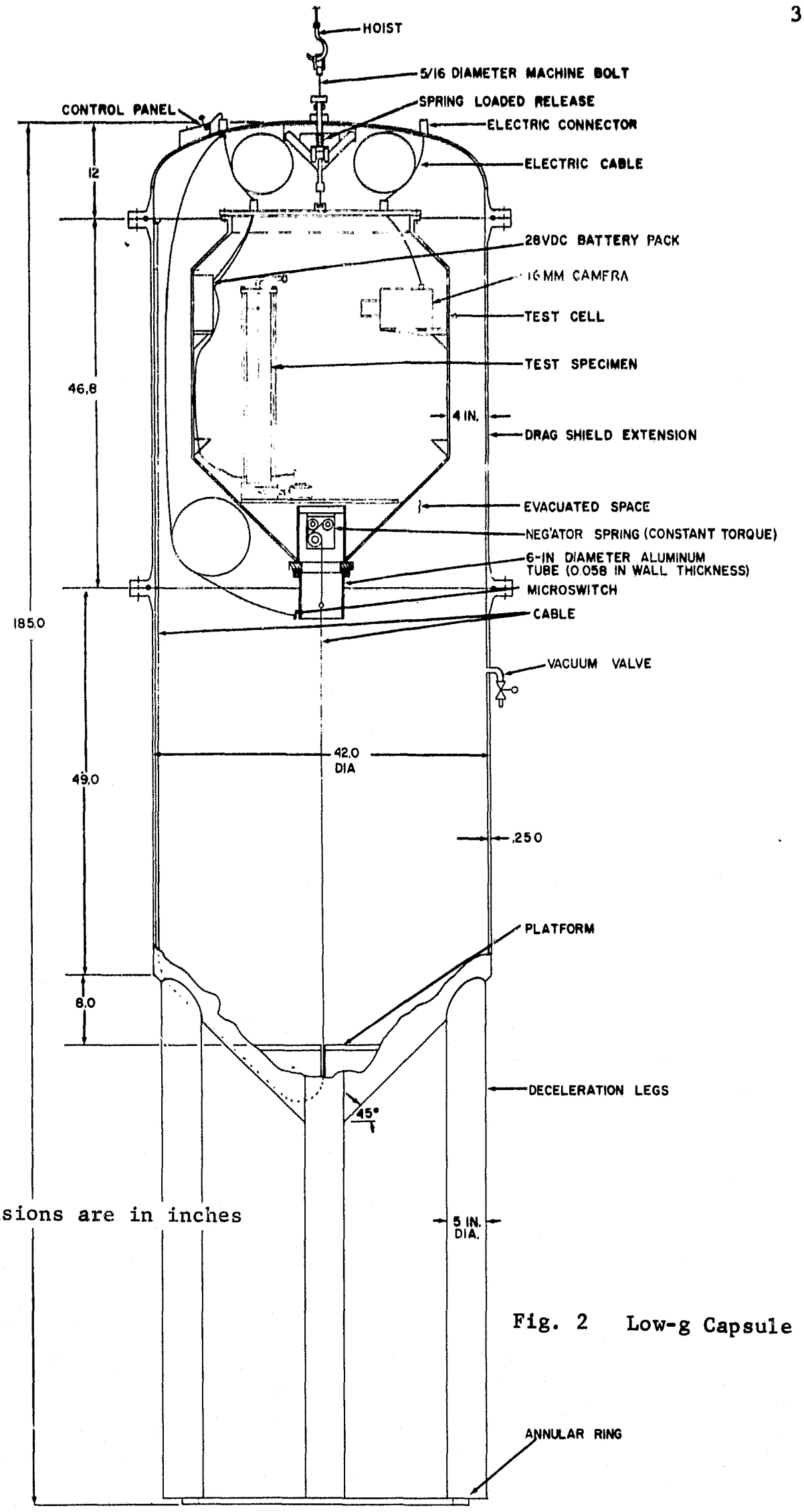

Note: Dimensions are in inches

Fig. 2 Low-g Capsule Assembly

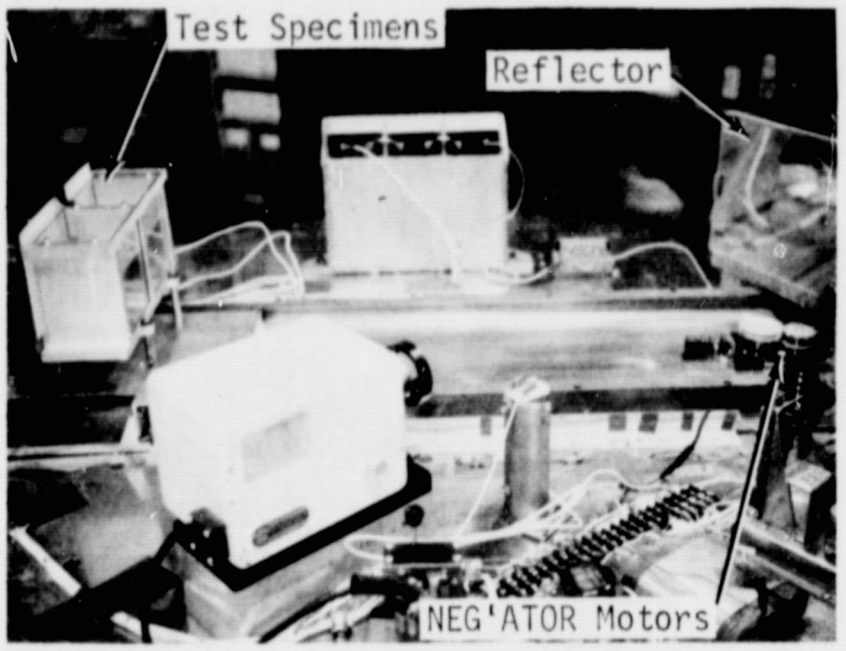

Fig. 3 Lateral Travel Mechanism

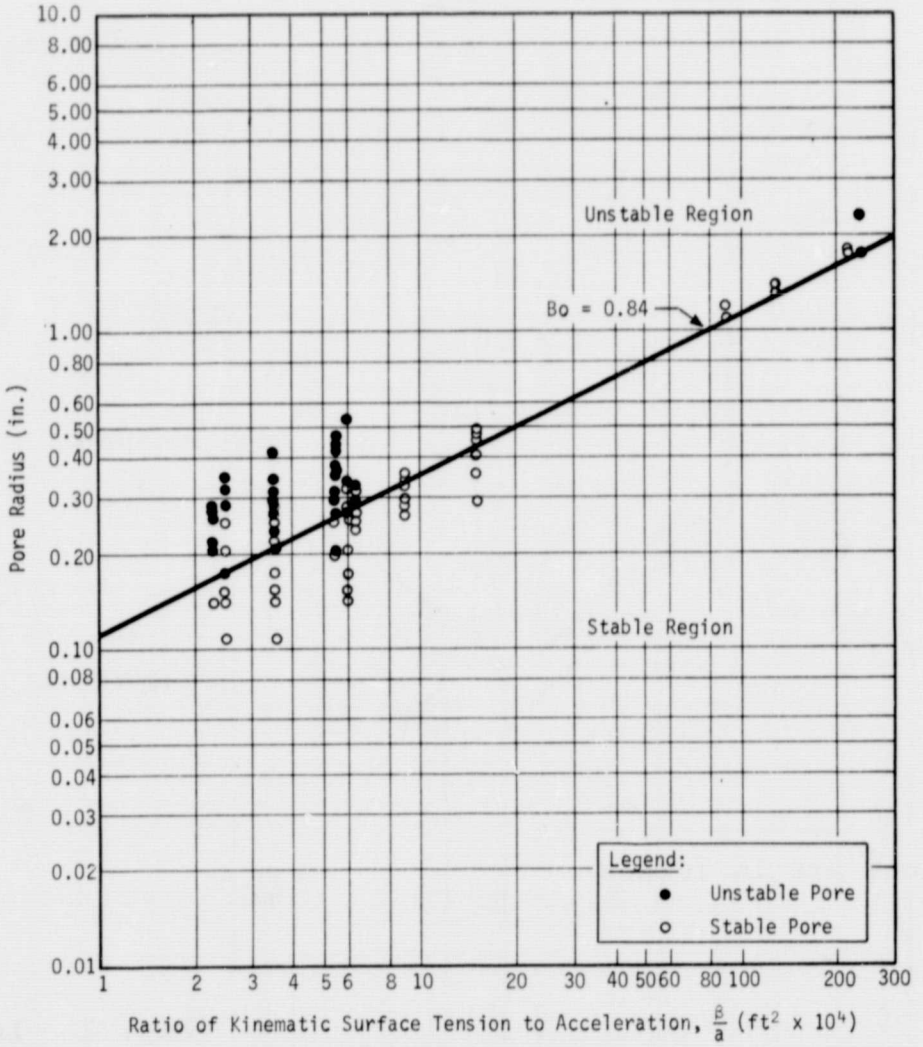

Fig. 4 Stability Characteristics of Perforated Plate Barriers

MCR-69-585

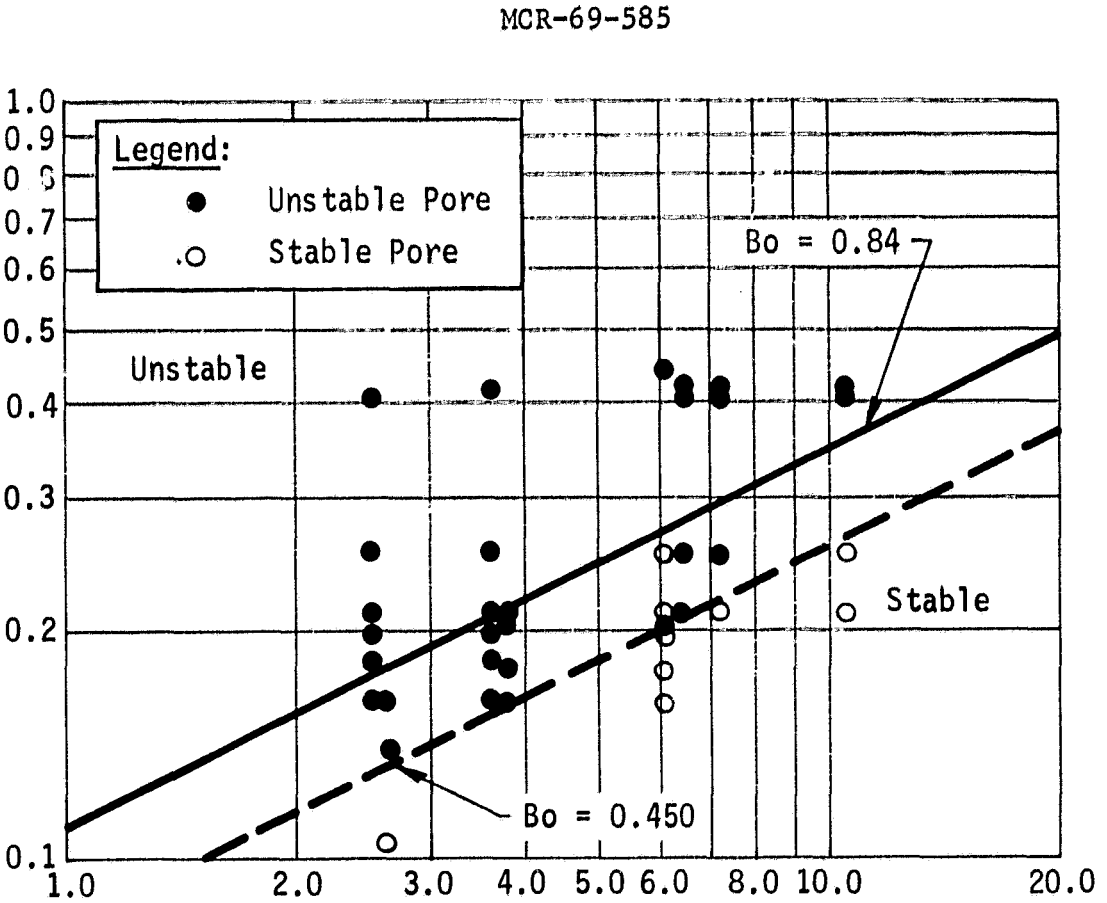

Fig. 5 Stability Characteristics of Square-Weave Screen Barriers

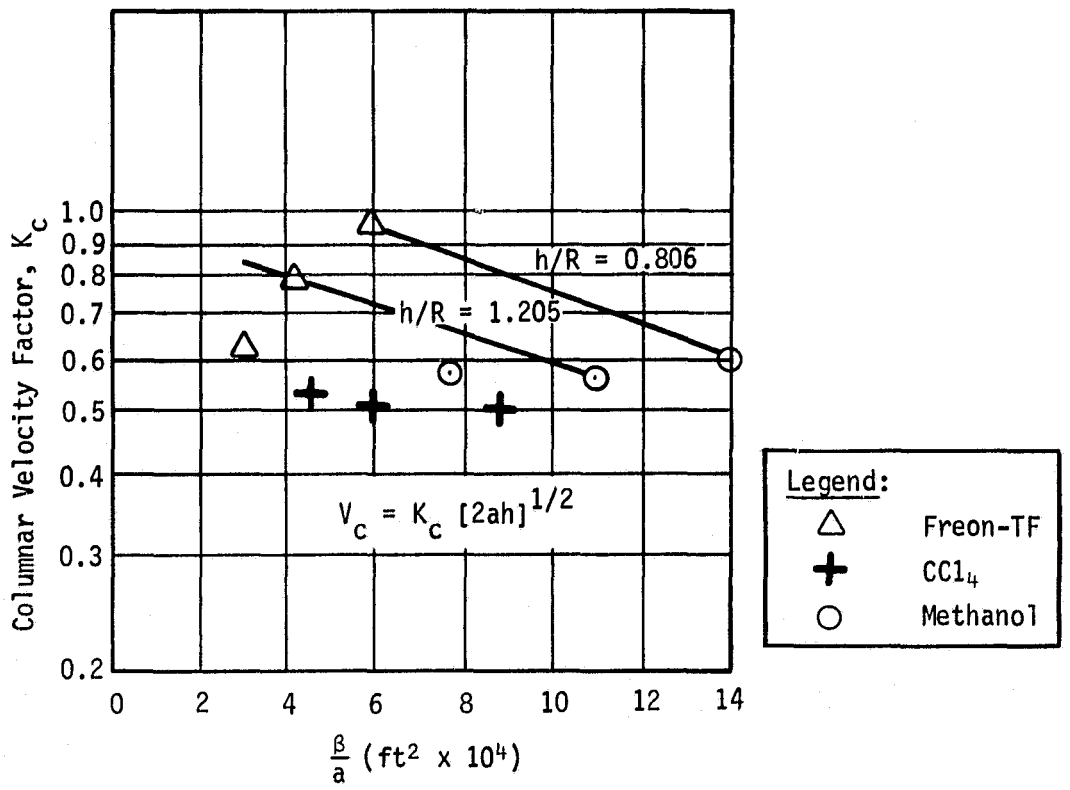

Fig. 6 Columnar Velocity Factor (K_c)

Category A

Category B

Category C

Category D

Category E

Category F or G

Fig. 7 Damping Categories A thru G

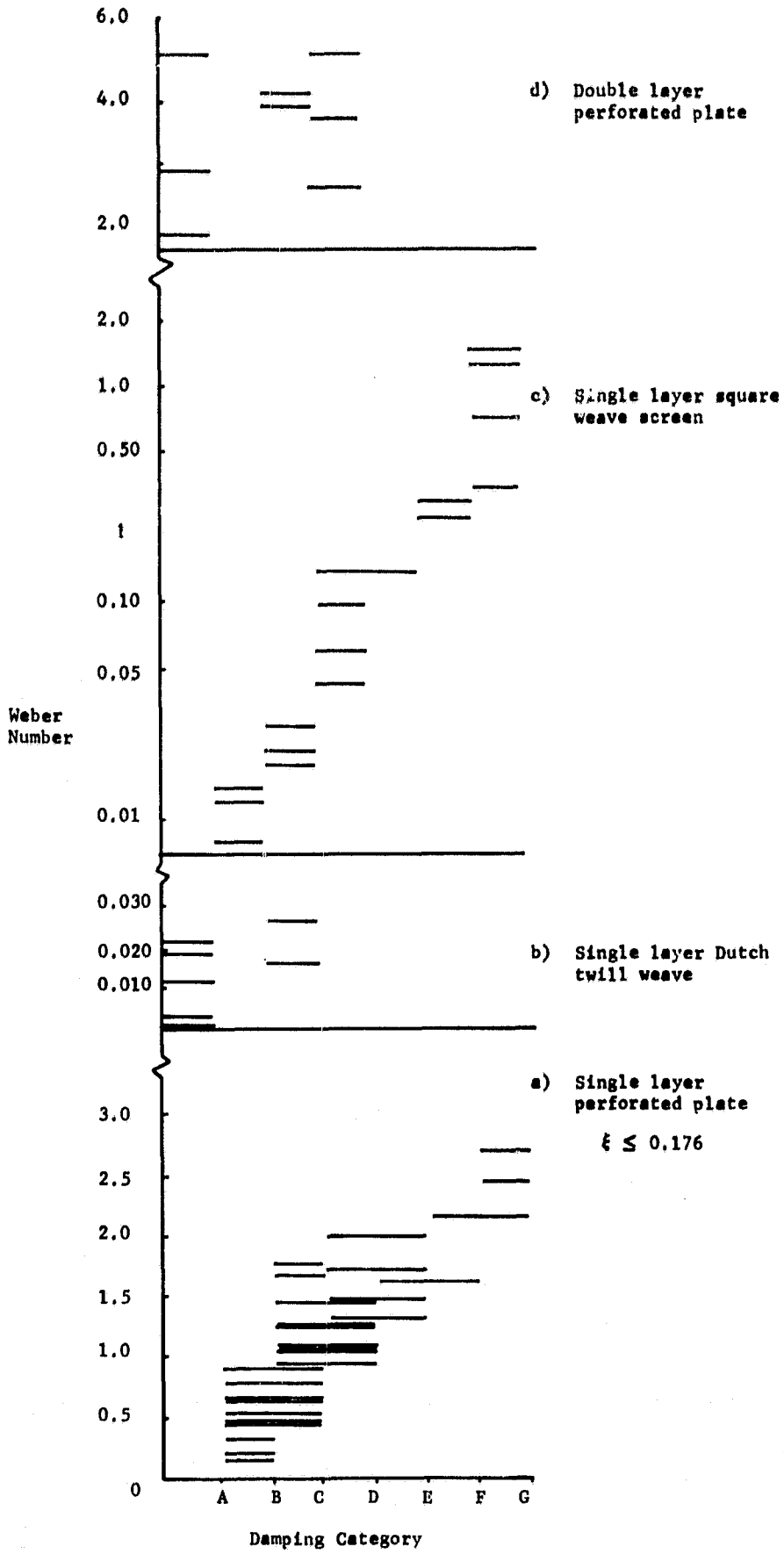

Fig. 8 Damping Performance of Selected Barriers

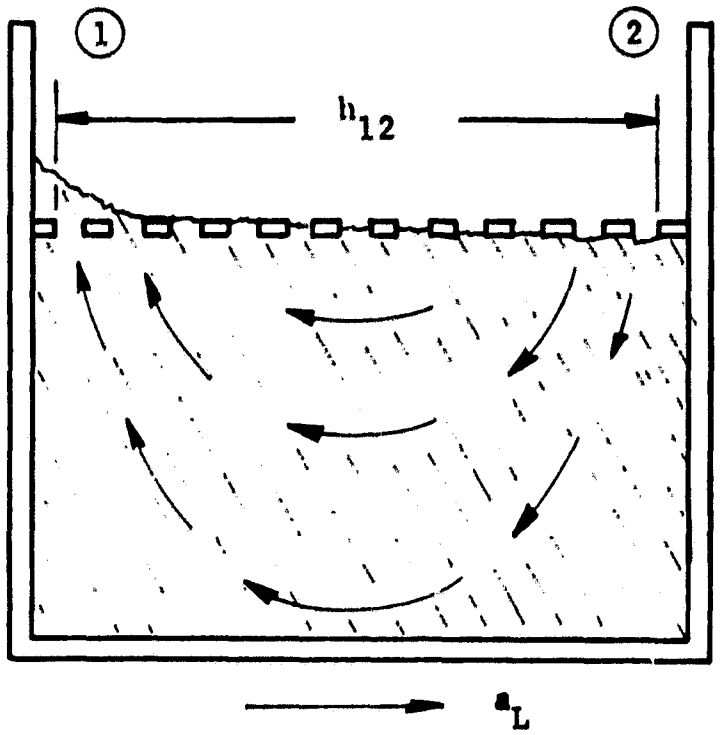

Fig. 9 Possible Sidewise Liquid Motion

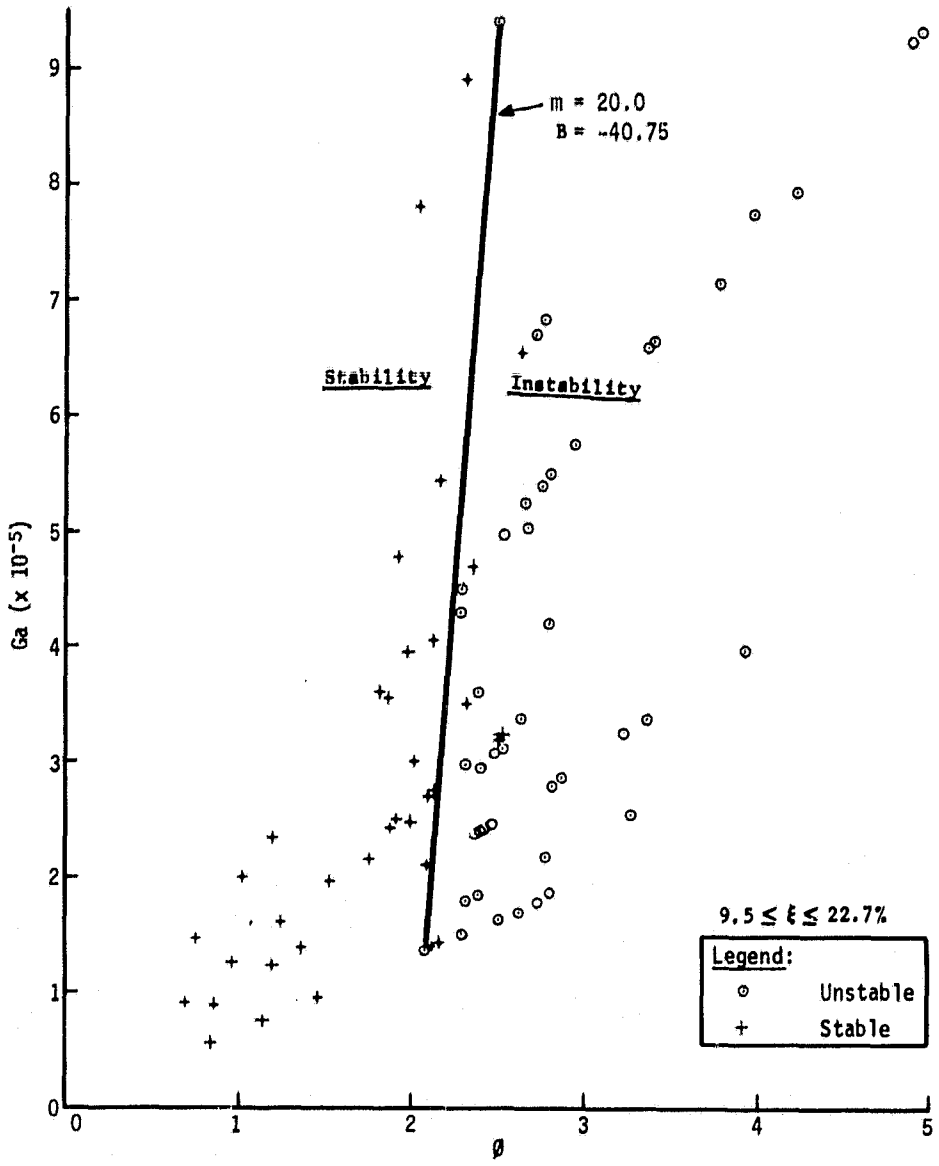

Fig. 10 Stability Criteria for Straight-Hole Perforated Plates

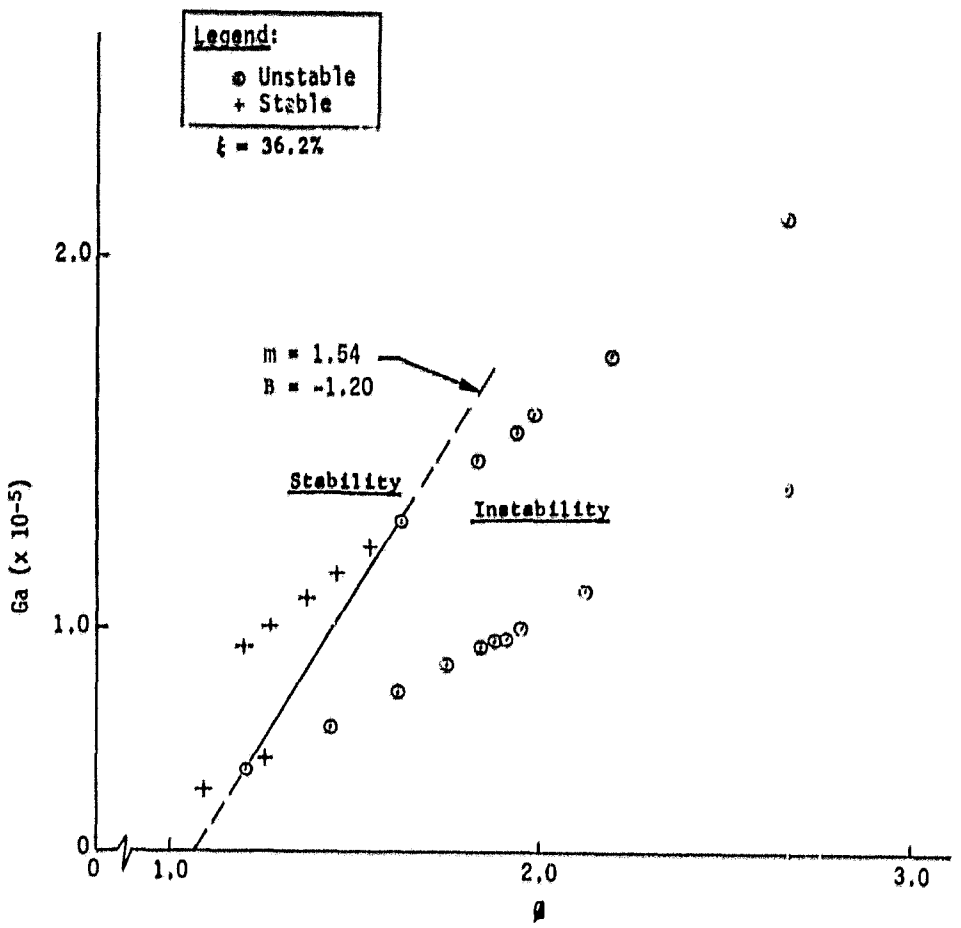

Fig. 11 Stability Criteria for Cone-Hole Perforated Plates

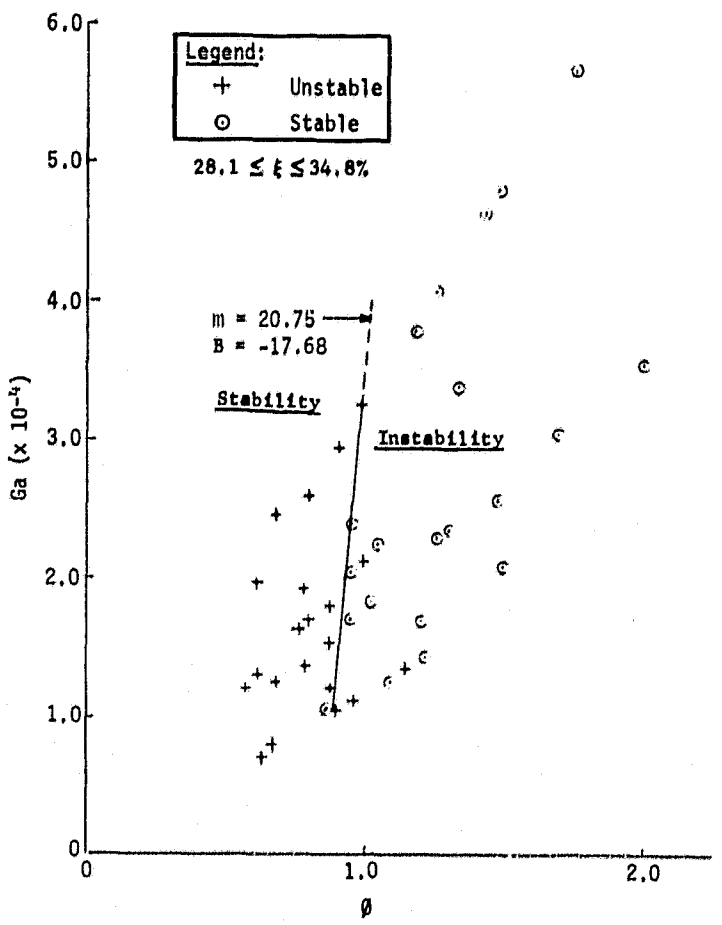

Fig. 12 Stability Criteria for Square-Weave Screen

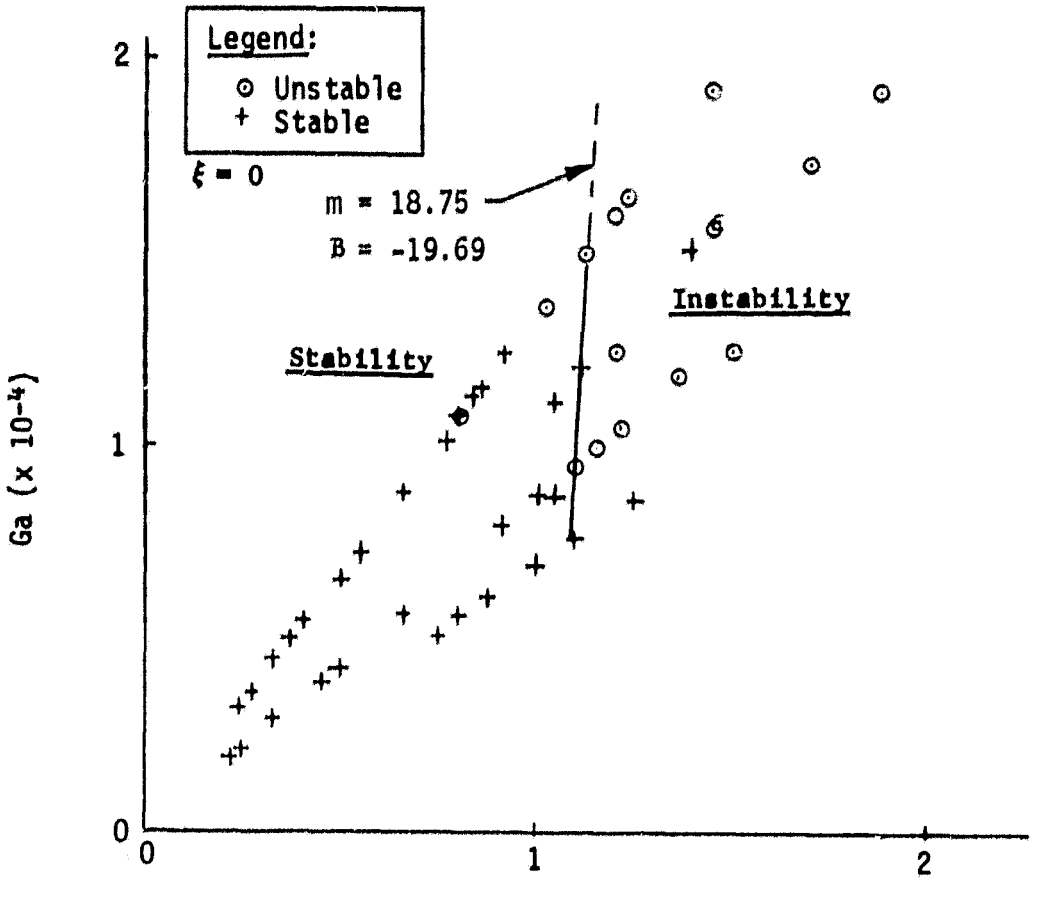

Fig. 13 Stability Criteria for Dutch-twill Cloth

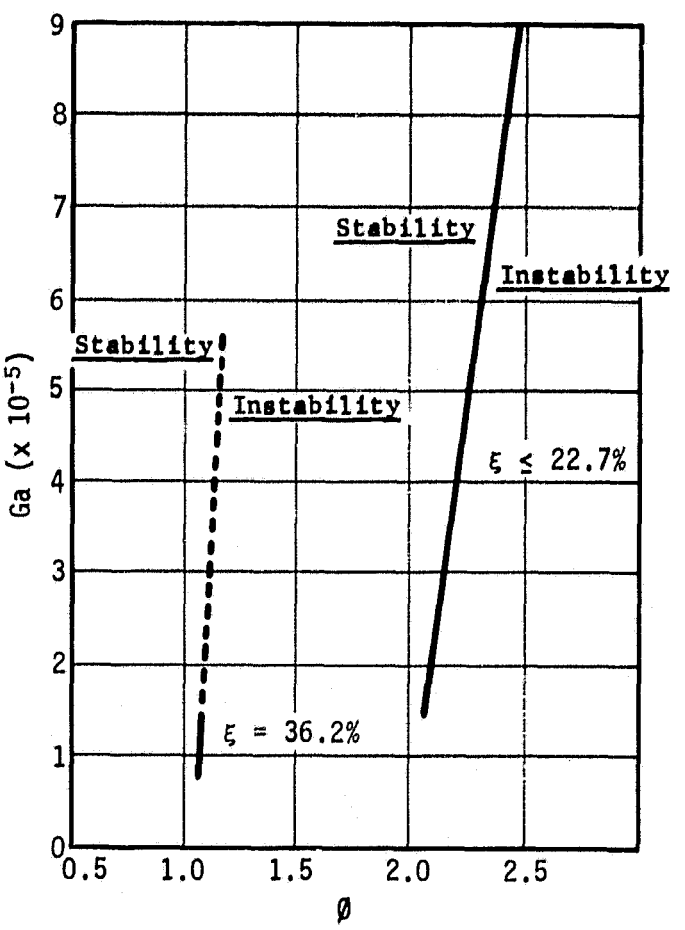

Fig. 14 Effect of Open-to-Closed Area Ratio on Stability of Perforated Plates

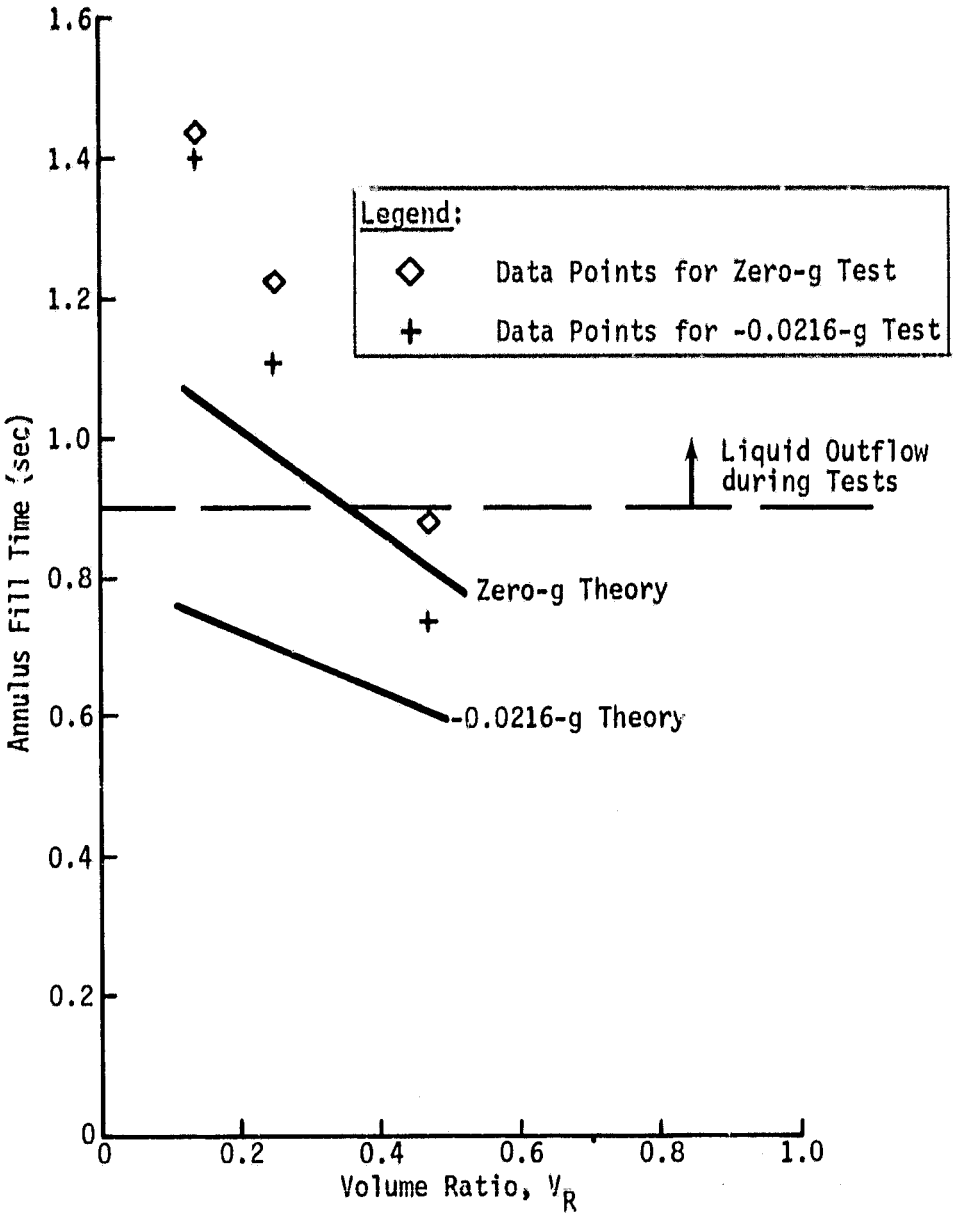

Fig. 15 Annulus Fill Time vs Liquid-to-Container Volume Ratio

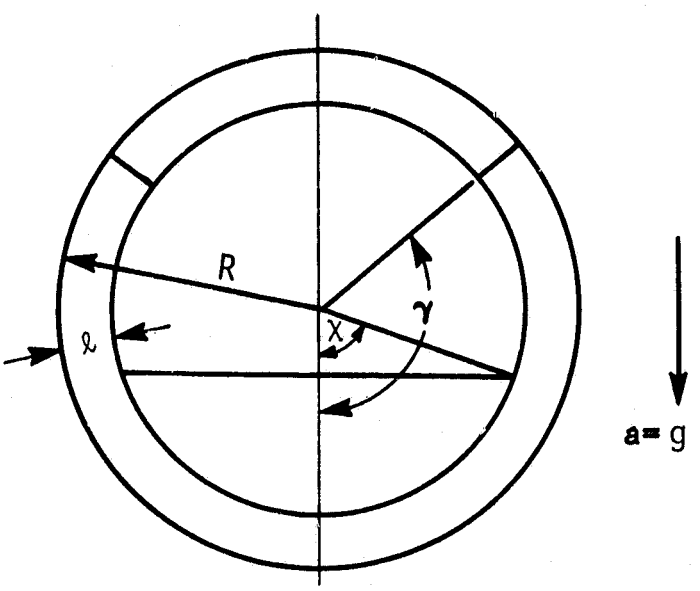

Fig. 16 Schematic Representation of Annulus Filling